Prediction of droplets characteristic diameters and polydispersity index induced by a bifluid spraying nozzle by the means of dimensional analysis

Kevin Lachin, M. Niane, M. Person, J. Mazet, G. Delaplace, C. Turchiuli

Prediction of droplets' characteristic diameters and polydispersity index induced by a bifluid spraying nozzle by the means of dimensional analysis

K. LACHIN[a*], M. NIANE[a], M. PERSON[b], J. MAZET[b], G. DELAPLACE[c], C. TURCHIULI[a]

[a] *Université Paris-Saclay, INRAE, AgroParisTech, UMR SayFood, F-91120 Palaiseau, France*

[b] *Soredab, F-78125 La Boissière-Ecole, France*

[c] *Univ. Lille, CNRS, INRAE, Centrale Lille, UMR 8207 - UMET - Unité Matériaux et Transformations, F-59000 Lille, France*

**Corresponding author: kevin.lachin@agroparistech.fr*

Highlights

- A rigorous dimensional analysis (DA) was performed on bifluid spray properties
- Two characteristic spray diameters and a polydispersity index were considered
- Models were established with conventional equation shapes and machine-learning (ML)
- Spray properties could be accurately modelled through a DA/ML approach
- Particle Size Distributions could also be predicted using this methodology

Abstract

This work focuses on the study of sprays generated through a bifluid nozzle and the modelling of characteristic spray properties (two characteristic diameters and a polydispersity index) using dimensional analysis. Two types of dimensionless models were identified for each spray target property from the 75 experimental points considered. The first type used a conventional monomial-exponential shape equation, and the second applied shape identification through machine-learning. Although conventional models of the first type were mostly satisfactory when considering the characteristic diameters, they nevertheless showed clear limitations addressed by the machine-learning identified models. The conventional approach also failed to identify a satisfactory equation for the polydispersity index. The machine-learning approach provided an equation identifying this index to the main dimensionless parameters governing atomization. This identification provides a foundation for proposing a two-parameters dimensionless model that predicts spray particle size distribution. The combination of dimensional analysis with machine-learning equation identification thus paves the way to physically rigorous and easy-to-use models capable of predicting characteristic properties and full distributions.

Keywords

Dimensional analysis; bifluid nozzle; droplet size distribution modeling; atomization; machine learning modeling

1. Introduction

Atomization remains essential in chemical engineering and is frequently used in many domains, functioning as a key step in processes such as, for example, fuel combustion [1] and probiotic encapsulation [2]. Atomization corresponds to the disintegration of a liquid in a surrounding gas that can be still or in motion. This disintegration occurs through a nozzle and generates a spray. This spray can then be used in its dispersed liquid form or transformed (frozen or dried) to obtain the product of interest. The dried usage is applied in spray-drying, where atomization is the first step in the formation of solid particles (e.g., for milk powder production).

Among the diversity of nozzles that can be employed, two categories are commonly used in industrial applications: pressure nozzles (where the fragmentation results from a kinetic energy dissipation inside the slots [3]) and bifluid nozzles (where atomization is air-assisted and comes from the shearing occurring at the air-liquid interface [4]). With both types of nozzles, two spray properties are particularly interesting in atomization: a characteristic diameter and the size distribution (PSD) of generated droplets. While the knowledge of a diameter gives general information about the spray quality (coarse or fine spray), the droplet size distribution itself is also of full relevance, especially in the case of spray-drying. The spray PSD will indeed directly impact that of the resulting powder particles as well as their behavior during drying with an impact on the final powder properties (flowability, packing properties, wettability) which are highly dependent on the PSD [5]. The prediction of these two spray properties is thus of great interest for the experimenter working with various fluids to efficiently pilot the atomization process to the needs.

Concerning characteristic diameter, “ready-to-use” correlations predicting diameters depending on fluid and process parameters flourish in the literature [4,6–9]. While of great interest and use in the parameter range in which they are established, these correlations however fail at representing the complexity of a size distribution. Generally speaking, when determining a PSD through modeling, Population Balance Equations (PBE) are often invoked to predict time-dependent and steady-state distributions of the dispersed medium [10,11]. While robust and efficient, PBE requires both kinetic information (aggregation/coalescence, rupture kernels) and computational power (especially when coupled with CFD) making them difficult to use effectively. Simple correlations capable of estimating a PSD, as it is the case for characteristic diameter, could thus be of great interest.

For such complex phenomena, dimensional analysis is an interesting tool to consider. Dimensional analysis is a methodology of prime importance in chemical engineering as it offers both a means to semi-empirically model complex phenomena for which full numerical approaches are too complex and time-consuming, and a way to qualitatively understand the prevalence of the phenomena at stake. Among some of the applications for which this approach is of high relevance, one can mention mass transfer in stirred tanks [12], mixing inside a novel mixing device [13], or size prediction when atomizing [4,6]. Recent developments in this field also proposed a method to combine design of experiments with dimensional analysis to optimize the number of experiments to be performed, with satisfactory preliminary results [14].

This article focuses on bifluid nozzle atomization, and specifically on establishing new correlations predicting characteristic diameters for the experimental bifluid setup of this study. These kinds of correlations already exist in the literature and use monomial/exponential terms. Unfortunately, they often lack precision due to the shape of the equation used. We will thus overcome this obstacle by proposing a comprehensive dimensional analysis study combined with a symbolic regression software for the identification of the best fitting equation shape. The results of both approaches

(monomial/exponential and symbolic regression) will be compared and discussed extensively. A methodology to quickly estimate the PSD of a spray depending on the fluid properties and operating conditions will then be proposed. This methodology relies on the liquid fragmentation theory proposed by Villermaux [15]. This theory leads to a two-parameters mathematical function describing the spray size distribution (a characteristic diameter and a polydispersity index). Dimensional analysis will be used to predict the parameters of this PSD function. The article concludes by discussing the robustness and utility of the PSD prediction.

2. Materials and methods

2.1 Sprayed liquids

Five mixtures of water-glycerol-ethanol were formulated based on the spraying experiments performed by Mandato et al. [6] in order to get five model liquids with a large variety of viscosity, surface tension and density (*Table 1*). Glycerol (CAS Number 56-81-5, purity ≥ 97%) was purchased from VWR Chemicals (Belgium) and ethanol (CAS number 64-17-5, purity = 96%) from Sigma Aldrich (USA). Type II deionized water was also used for the mixtures.

Glycerol was mainly used in this study to change the dynamic viscosity of the solutions. Ethanol was also added in solutions 4 and 5 in order to tune the surface tension while keeping dynamic viscosities almost identical to those of solutions 2 and 3. These formulations were also chosen to ensure adequate liquid flowrate when pumping and user safety (relative to the spraying of ethanol) when performing the experiments. The results obtained with the five solutions were afterwards used to feed the dimensionless models proposed and identify the correlations (training data set). The robustness of the models was afterwards tested using a 30% w./w. reconstituted skimmed milk solution (validation data set). The milk powder used for reconstitution was bought from a local store (Cora, France). Skimmed milk is a product of particular relevance for this study, as it exhibits a Newtonian behavior [4] while being widely used industrially to produce milk powder with spraying nozzles.

Table 1 : Composition and physical properties at 20°C of the sprayed liquids

Solution	**% Water** *(w./w.)*	**% Glycerol** *(w./w.)*	**% Ethanol** *(w./w.)*	**μ** *(mPa.s)*	**ρ** *($kg.m^{-3}$)*	**σ** *($mN.m^{-1}$)*
1	100	0	0	1.1	998	65.1
2	20	80	0	58.4	1200.6	59.8
3	15	85	0	107.0	1202.3	58.6
4	14.75	75.25	10	55.5	1147.6	35.8
5	9.9	81.1	9	107.3	1162.2	36.3
Milk (30% w./w.)	-	-	-	18.7	1105	41.9

The viscosity, density, and surface tension of the liquids used (*Table 1*) were estimated as follows. The dynamic viscosity and Newtonian behavior of the solutions was experimentally assessed on a Anton Paar MCR 301 (Anton Paar, Austria) rheometer by varying the shear rate between 1 and 200 s^{-1} with a

logarithmic ramp of duration 320 s inside a Couette geometry. The measurements were performed at a temperature of 20°C (spraying experiments temperature) in triplicate. Liquid density ρ_l was also determined three times by measuring the mass corresponding to 10 mL of solution at 20°C with a scale of precision +/- 0.001 g. Ultimately, surface tension σ at equilibrium was measured in triplicate on a Teclis tensiometer (Teclis Scientific, France) using the rising drop method. The maximal coefficients of variation assessed were respectively 1.4%, 0.16%, and 0.82% for the dynamic viscosity, density, and surface tension measurements.

2.2 Spraying set-up and process conditions explored

2.2.1 Bifluid nozzle and related geometrical parameters

The nozzle used for the experiments was a co-current bifluid nozzle with external mixing (Minor Mobile bifluid nozzle, GEA, Germany), as presented in *Figure 1*. Characteristic diameters of the nozzle (d_l, $d_{a,int}$, $d_{a,ext}$) were measured using the software Image J on nozzle cap snapshots taken with an optical microscope. These measurements were done three times, and the average measured values are reported in *Table 2*.

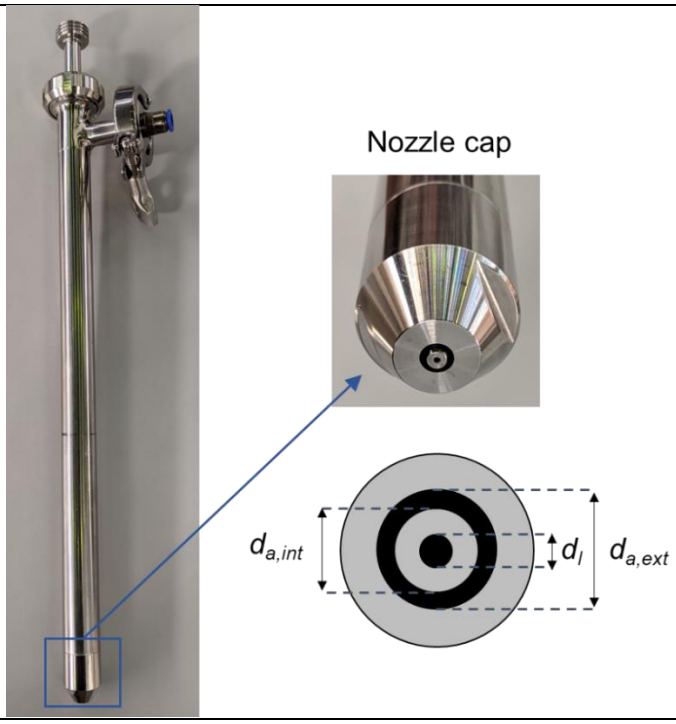

Figure 1: Bifluid nozzle used with the pilot set-up

Table 2: Nozzle geometric parameters value with coefficient of variation over 3 measurements

	d_l	$d_{a,int}$	$d_{a,ext}$
Value (mm)	1.06	3.62	4.97
Var coef. (%)	0.55	0.69	0.12

2.2.2 Pilot set-up and process operating conditions

The pilot-scale set-up used for the experiments is detailed in *Figure 2*: Spraying and image acquisition set-up. The sprayed solutions were firstly mechanically stirred inside a double-jacketed tank of volume V = 5 L thermally regulated at T = 20°C. The liquid flowrate inside the nozzle was set by a peristaltic pump (Masterflex L/S -EasyLoad head pump, Cole-Parmer, USA), and the mass liquid flowrate was calculated using a scale recording the mass variation through time when spraying. Air volumetric flowrate was imposed with a manual gas flowmeter (FR4500 Gas flowmeter, Key Instruments, USA) and air properties (temperature and humidity) were systematically controlled before spraying. The corresponding air density value used for the calculation was ρ_a = 1.204 kg.m^{-3}.

A vacuum system was also set up to avoid as much as possible spray visualization issues (mist accumulation inside the experiment room, droplet deposal on the camera, spurious recirculation of drops in the camera field of observation). Tests were performed before the experimental campaign and showed that this system does not disturbs the liquid flow at the measurement position.

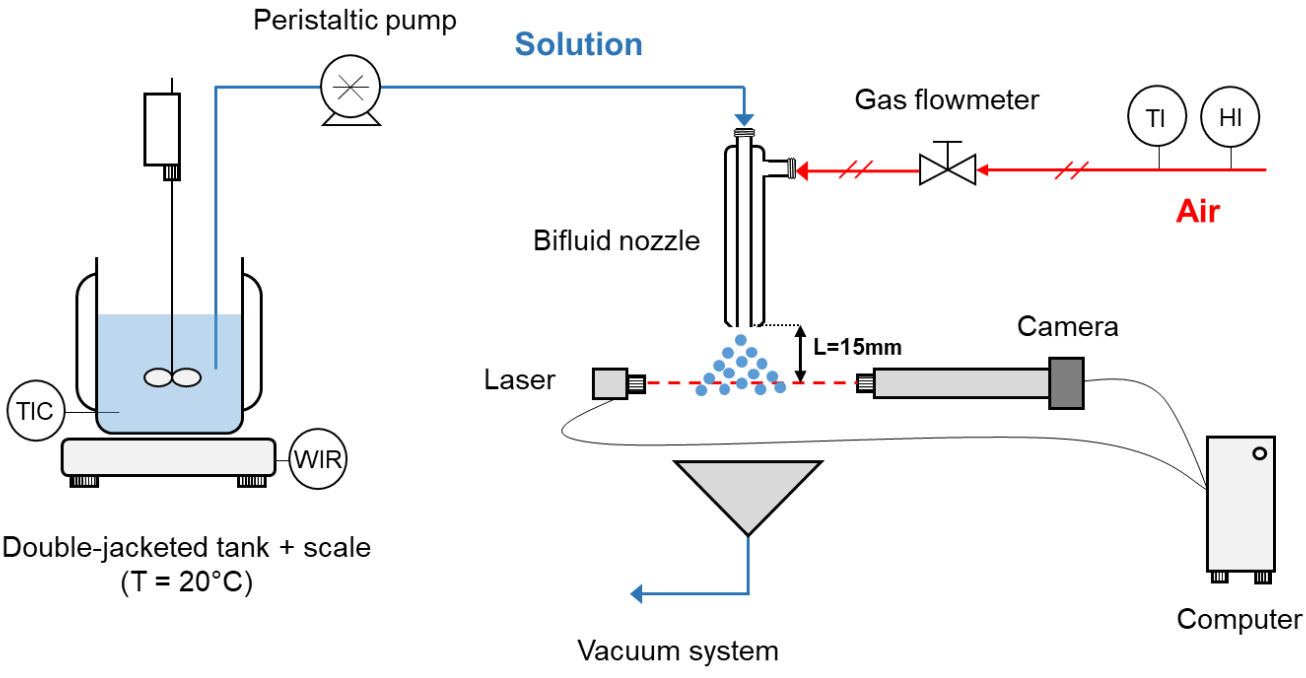

Figure 2: Spraying and image acquisition set-up

Table 3 summarizes the process conditions explored for each of the six solutions during the experimental campaign. Three air flow rates were investigated per solution, and five liquid flowrates were swept per air flowrate considered. In total, 15 experimental points per fluid were thus obtained, leading to 75 experimental points for the training data set and 15 for the validation data set (reconstituted skimmed milk). The maximal flowrate achievable with a peristaltic pump is highly influenced by the liquid dynamic viscosity. For the solutions with the highest viscosity (solutions 3 and 5), the mass flowrate range explored was thus of a lesser magnitude than for the other four solutions.

Table 3: Air and sprayed liquid flowrate values chosen for atomization experiments (20°C)

Solution	Liquid mass flowrates *($g.min^{-1}$)*	Air volumetric flowrates *($L.min^{-1}$)*
1	50; 90; 130; 170; 210	90; 110; 130
2	50; 90; 130; 170; 210	90; 110; 130
3	50; 70; 90; 110; 130	90; 110; 130
4	50; 90; 130; 170; 210	90; 110; 130
5	50; 70; 90; 110; 130	90; 110; 130
Milk (30% w./w.)	50; 90; 130; 170; 210	90; 110; 130

2.3 Image acquisition and exploitation

2.3.1 Image acquisition

Images of the sprayed droplets were recorded using a laser image acquisition system designed by R&D Vision (R&D Vision, France), allowing to capture images of a maximum resolution 3296*2472 pixels with a maximal 16 Hz frequency. The acquisition camera (VA-8M, Vieworks, South Korea) is synchronized with a pulsed laser of wavelength 640 nm to illuminate the zone to photography. The laser and camera were mounted on a metallic frame whose position can be adjusted on the X, Y, and Z axes through micromotors (A-LST, Zaber Technologies, Canada), ensuring a precise and reproducible camera position.

The acquisition was performed at a distance *L* = 15 mm from the nozzle outlet. At this position, steady-state was experimentally observed after a few seconds. The acquisition was thus triggered after spraying for 30 seconds (to ensure steady-state) and made for another 30 seconds. Approximately 400 processed images per operating condition were recorded. *Figure 3* shows examples of images obtained when spraying solution 2 in two operating conditions: air volumetric flowrate = 90 $L.min^{-1}$ - liquid mass flowrate = 50 $g.min^{-1}$ (left) and air volumetric flowrate = 90 $L.min^{-1}$ - liquid mass flowrate = 90 $g.min^{-1}$ (right).

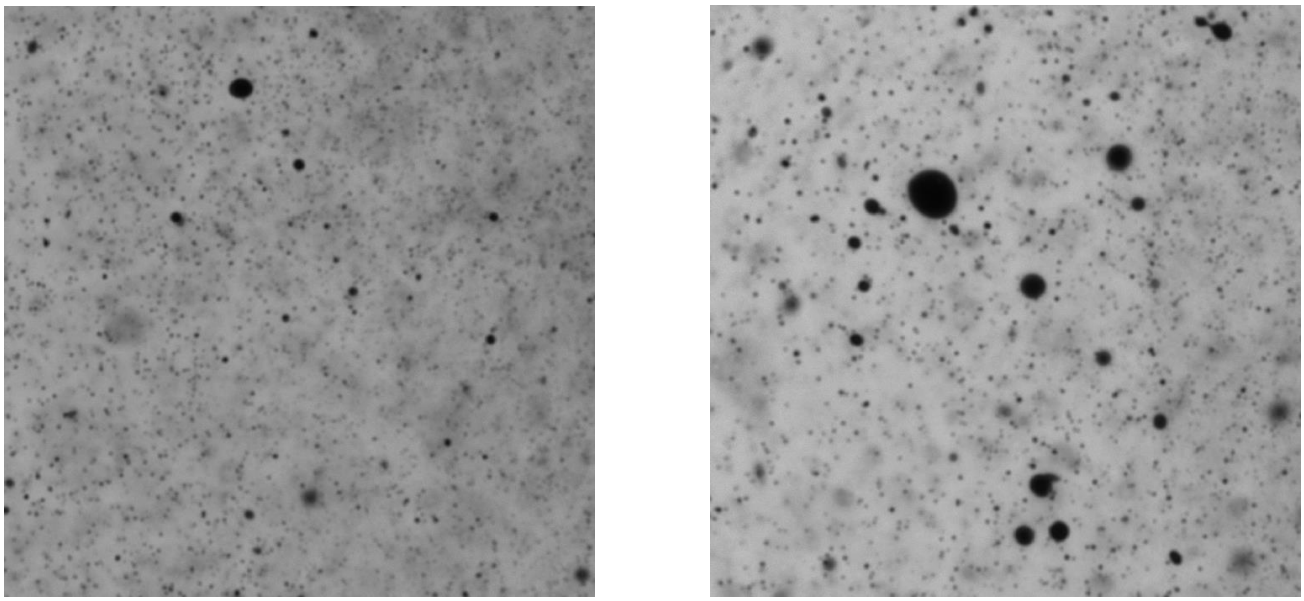

Figure 3: Example of images acquired during spraying of solution 2. Left: air flowrate = 90 L.min^{-1}, liquid flowrate = 50 g.min^{-1}; right: air flowrate = 90 L.min^{-1}, liquid flowrate = 90 g.min^{-1}

2.3.2 Data treatment and statistical analysis

Each image obtained was then processed using the software HIRIS 5.1.4 (R&D Vision, France) to determine the diameter of each droplet in the observation field. Drops lying outside the depth of field (blurred) or appearing superimposed or only partially on the images were automatically eliminated using shape and contrast filters. *Figure 4* shows an example of the result of image processing using HIRIS after selecting the right set of filters. For clarity concerns, only a fraction of the treated image is presented in this figure. Among all the particles in the initial picture (on the left), only the ones circled in red on the processed image (on the right) were taken into account by the software.

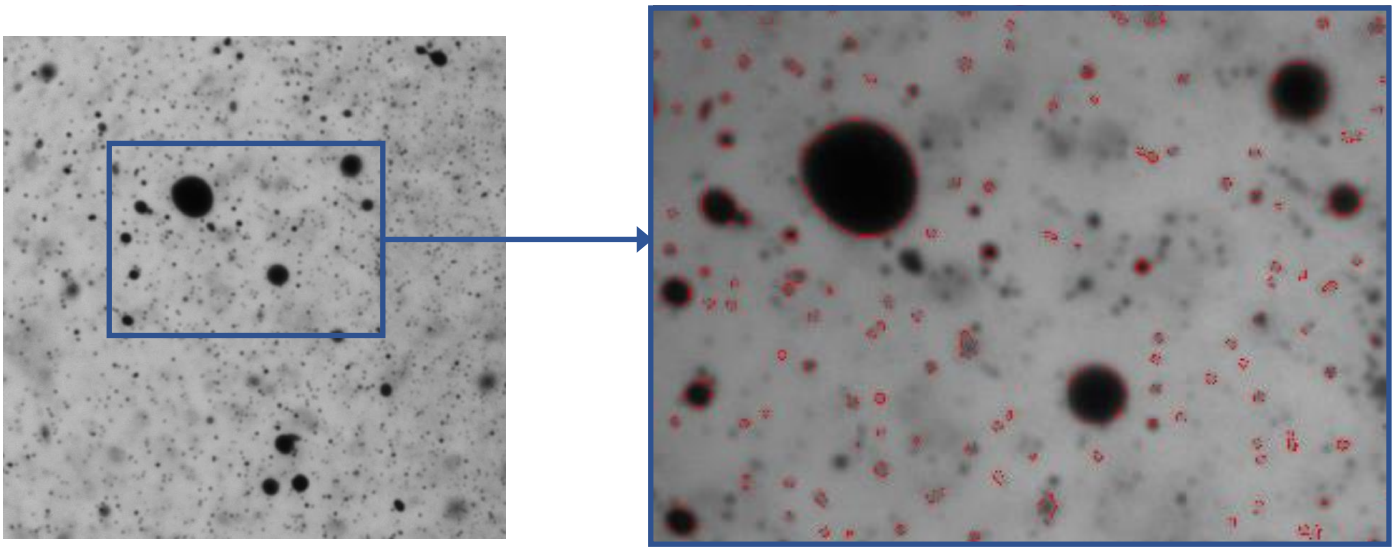

Figure 4: Example of HIRIS image processing

The diameter of each droplet considered by image processing was calculated from the measured surface area as the equivalent sphere surface diameter. To naturally account for the instantaneous acquisition variability in the final values used, we calculated the characteristic diameter and size distribution for each single spraying condition by gathering all the particles analyzed on the 400 images.

The subsequent calculations and optimizations were performed using the matrix calculation software MATLAB (MATLAB 9.4.0.813, MathWorks, USA). We respectively used *fminsearch*, *integer, diff,* and *interp1* functions for least-squares optimization, numerical integration, differential calculation, and linear data interpolation. Monomial and exponential relations were linearized applying logarithm, allowing coefficient identification from the experimental data through a multiple linear regression based on the singular value decomposition method (function *fitlm*). The calculated coefficients significance was assessed through a Student test. The variance analysis was also checked to follow a F test. The machine-learning software Eureqa was used to identify relations through symbolic regression algorithms. The input variables selected for the symbolic regression were the set of experimental dimensionless numbers identified by the dimensional analysis (detailed in *3.2*). All basic mathematical functions were considered, so as exponential, root-square, logarithm and power functions. Trigonometric functions were however not considered because very unlikely to seize the physics at stake. Among the relation shapes estimated by the software, we systematically kept the equation with the smallest number of coefficients as the increase in complexity in the equations identified by the software did not brought significant improvements in terms of fitness quality (R^2 value), while making the equation less easy to use.

3. Dimensional analysis

A correct and comprehensive dimensional analysis must follow some rules to be correctly established. The dimensional analysis presented in this study thus strictly follows the steps described by Delaplace et al. [16] :

- Listing of the independent parameters/variables related to the target parameter;
- Determination of the dimension of each parameter in terms of fundamental dimensions;
- Application of the Vashy-Buckingham theorem;
- Construction of the resulting dimensionless numbers;
- Eventually, reorganization of these numbers to make appear more relevant ones.

3.1 Target variable and related parameters

When it comes to atomization, the main information the experimentalist usually needs to estimate is a characteristic diameter of the droplet size distribution. In order to detail the mathematical process employed in a generic way, a characteristic droplet diameter d_{char} is introduced in the subsequent sections. This characteristic diameter will be impacted by several parameters and variables:

- Material-related variables (sprayed liquid and air, at 20°C): ρ_l, ρ_a, μ_l, μ_a, σ;
- Process-related variables: u_l, u_a, L;
- Nozzle geometric parameters: d_l, $d_{a,int}$, $d_{a,ext}$;

- Physical constants: *g.*

Among the process-related variables, L (the distance between the nozzle outlet and the position where the droplet size is measured) must be taken into consideration since droplet fragmentation and coalescence phenomena may occur in the spray.

Assuming that the variables and parameters of influence are extensively listed, one can then state the existence of the following relation, where *f* stands for an unknown function (*Equation 1*):

$d_{char} = f(\rho_l, \rho_a, \mu_l, \mu_a, \sigma, u_l, u_a, L, d_l, d_{a,int}, d_{a,ext}, g)$	*Equation 1*

This relation will subsequently be simplified by making appear relevant dimensionless numbers and removing the constant parameters.

3.2 From dimensions to relevant dimensionless numbers

The above-mentioned parameters embody three fundamental dimensions: the mass dimension M, the length dimension L, and the time dimension T. The corresponding dimensional matrix is presented in *Table 4*.

Table 4: Dimension matrix D, with central matrix C (dark grey) and Residual matrix R (white)

	d_{char}	ρ_l	ρ_a	μ_l	σ	u_l	u_a	d_l	$d_{a,int}$	$d_{a,ext}$	μ_a	L	g
M	0	1	1	1	1	0	0	0	0	0	1	0	0
L	1	-3	-3	-1	0	1	1	1	1	1	-1	1	1
T	0	0	0	-1	-2	-1	-1	0	0	0	-1	0	-2

The repeated variables used in this study (μ_a, *L*, and *g* in the central matrix) were chosen accordingly to Petit et al. [4], which demonstrated the relevance of such a base while studying a similar atomization set-up. When applied, the Vashy-Buckingham theorem gives the relation between dimensionless numbers presented by *Equation 2*, where *F* stands for the mathematical function relating the causal dimensionless numbers to the target dimensionless number d_{char}/L.

$\frac{d_{char}}{L} = F\left(\frac{\rho_l}{\mu_a.L^{-1.5}.g^{-0.5}}, \frac{\rho_a}{\mu_a.L^{-1.5}.g^{-0.5}}, \frac{\mu_l}{\mu_a}, \frac{\sigma}{\mu_a.L^{0.5}.g^{0.5}}, \frac{u_l}{L^{0.5}.g^{0.5}}, \frac{u_a}{L^{0.5}.g^{0.5}}, \frac{d_l}{L}, \frac{d_{a,int}}{L}, \frac{d_{a,ext}}{L}\right)$	*Equation 2*

These initial dimensionless numbers can afterward be rearranged to make appear more intuitive dimensionless numbers regarding the phenomena studied. In this case, the aerodynamic Weber number *We (Equation 3)*, the Bond number *Bo* (*Equation 4)*, and the Air-to-Liquid Ratio *ALR* (*Equation 5*) were chosen as of particular relevance when studying atomization:

$We = \frac{\rho_l (u_a - u_l)^2 d_l}{\sigma}$	*Equation 3*

$Bo = \frac{(\rho_l - \rho_a).g.d_l^2}{\sigma}$	*Equation 4*

$ALR = \frac{\dot{m}_a}{\dot{m}_l} = \frac{\rho_a.({d_{a,ext}}^2 - {d_{a,int}}^2).u_a}{\rho_l.{d_l}^2.u_l}$	*Equation 5*

At low viscosity, the deformation of a drop inside an air stream is mostly controlled by the aerodynamic and surface tension forces. The ratio between these forces leads to the expression introduced in *Equation 3* (Weber number) that compares process conditions to the physico-chemical properties of the liquid sprayed. Due to its nature, the Weber number is naturally used in a lot of studies involving droplets. The higher the *We* value, the more the deforming aerodynamic forces overcome the reforming surface tension forces, ultimately leading to smaller droplets [17].

The Air-to-Liquid Ratio (*ALR*), also called Gas-to-Liquid Ratio, is defined as the ratio between the air and liquid mass flowrates. This dimensionless number is of typical use in the case of bifluid atomization, and frequently considered in droplet atomization models as it embodies the influence of the atomization process conditions [17,18]. The higher the ALR, the smaller the droplets generated.

The Bond number *Bo* is also commonly used when studying bubbles and drops as it allows their shape characterization. By comparing the gravitational forces to the surface tension ones (and thus measuring the influence of surface tension independently of the process conditions, unlike *We*), this number also gives an indication of the influence of the surface tension on the flow studied [19].

Extensive details of the mathematical operations leading to *Equation 2* can be found in a previous article [3], and the extensive number reorganization giving birth to *We*, *Bo*, and *ALR* is detailed in the work of Petit et al. [4]. The work presented in this article focuses on a single nozzle geometry. The dimensionless numbers $\frac{d_l}{L}, \frac{d_{a,int}}{L}, \frac{d_{a,ext}}{L}$ are thus constant. Also, $\frac{\rho_a}{\mu_a.L^{-1.5}.g^{-0.5}}$ is constant as we did not consider any variation in the air properties and position of the observation zone. The relation between the ten dimensionless parameters introduced in *Equation 2* thus simplifies to the relation between six parameters depicted in *Equation 6*:

$\frac{d_{char}}{L} = F'(Bo, \frac{\mu_l}{\mu_a}, ALR, We, \frac{\rho_l}{\rho_a})$	*Equation 6*

3.3 Shape of the process relation and range of the numbers considered

When established, the dimensionless numbers are related through the Vashy-Buckingham theorem. However, the theorem does not state the shape of the relation between the parameters. When this relation is not known, a monomial function (that minimizes the number of constants to identify) is usually considered [20]. This equation shape is widely found in chemical engineering studies (as for example, when studying foaming ability of surfactants in a mechanical stirrer [20], axial dispersion in a rotary kiln [21]…). Sometimes, a combination of monomial and exponential terms can also be found in the literature [6]. When it comes to atomization, the dimensional analysis models proposed by Mandato et al. [6] and Petit et al. [4] are among the most comprehensive that currently exists. The authors respectively used monomial-exponential relation and fully monomial relation for their models. For this reason, we considered monomial and exponential terms for the conventional approach. More specifically, we used monomial terms for all the dimensionless numbers to identify characteristic diameters, except for *We* which influence was found to be better seized by an exponential term. For these correlations, coefficient identification was performed through multilinear regression after applying logarithm.

The overall range explored for the established dimensionless number in the conditions of this study is presented in *Figure ,* which also indicates the range of validity of the established correlations.

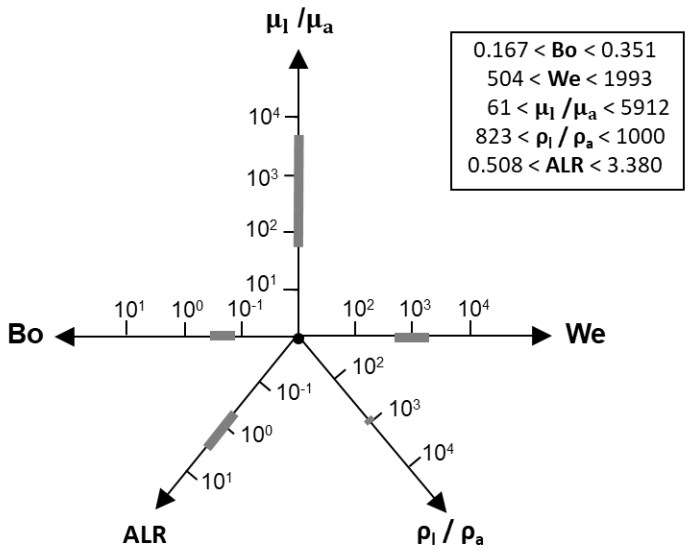

Figure 5: Dimensionless number range explored

4. Results

Based on the experimental results of the spraying trials with model solutions and reconstituted skimmed milk, different models were identified to characterize the liquid spray.

Sections *4.1* and *4.2* are dedicated to the identification of the correlation presented in *Equation 6* in the case of two characteristic diameters of frequent use: the median volumetric diameter $d_{v,50}$ and the average number diameter $d_{n,av}$. The grey dots in the subsequent figures (75 experimental conditions) represent the results obtained with the spraying of water-ethanol-glycerol mixtures (solutions 1 to 5, extensively presented in *Table 1*) under the process conditions introduced in *Table 3*. The grey dots are used to identify the equations proposed. The red dots correspond to the results obtained when spraying reconstituted milk (15 points), which are used as model validation points.

Section *4.3* is dedicated to the prediction of the droplet size distribution. First, in Section *4.3.1*, the atomization physical ground detailed by Villermaux is introduced. Then, using this theory, sections *4.3.2* and subsequent discuss a strategy to model a size probability distribution through dimensional analysis.

4.1 Median volumetric diameter correlations

The median volumetric diameter $d_{v,50}$, also called mass median diameter (MMD) can be defined as the diameter under which half of the total volume (or mass) of the sample is accumulated. A first modelling attempt for this diameter was performed with the 75 results obtained spraying the five model solutions (trained data), taking into account all the dimensionless numbers introduced in *Equation 6*. However, the *p-value* of the coefficient associated to the density ratio $\frac{\rho_l}{\rho_a}$ turned to be higher than 0.05, making this variable statistically insignificant. The narrow density ratio range explored here (*Figure*) might explain why the model is not able to convey a clear influence of this parameter over the results. The same density ratio insignificance was found by Petit et al. [4] with the

model established at the smallest distance from the nozzle. The authors explain that at small distances from the nozzle, physico-chemistry might not have a significant impact on the atomization process. We consequently chose to remove the density ratio from the dimensionless parameters of interest for the $d_{v,50}$ modelling. Coefficient identification on the correlation led to *Equation 7*, with corresponding adjusted coefficient of correlation $R^2 = 0.85$ and root-mean-square error RMSE = 0.0009:

$\frac{d_{v,50}}{L} = 0.001 * (Bo)^{0.98} * \left(\frac{\mu_L}{\mu_A}\right)^{0.14} . (ALR)^{-0.52} . e^{-5.3*10^{-4}.We}$	*Equation 7*

The adjustment between the experimental data and the estimated values are graphically represented on *Figure 6*, with dashed lines corresponding to the +- 20% relative error interval. The magnitude of the coefficient associated to each dimensionless number gives some essential guidance about the phenomena' prevalence in this process. Process related numbers (*ALR* and *We*, including the air and liquid velocities) have a significant impact on the diameter calculation: the higher these velocities-related numbers, the lower the droplet diameter. This result is expected, considering that the main rupture driving force in this type of nozzle is the liquid shearing through the air flow. Nevertheless, it is surprising to see that the fluid-related numbers (viscosity ratio for the liquid viscosity and Bond number for the surface tension) have such a high impact on the diameter, particularly the Bond number. Two reasons for this high impact can be invoked. The first reason is related to the distance *L* considered in this study, relatively close to the nozzle outlet (15 mm). At this distance and depending on the conditions, the liquid ligaments might not be fully sheared. In that case, it would not be surprising that liquid physico-chemical properties would still have a significant impact on the average droplet size. The second possibility is linked to the air volumetric flowrate values chosen. The lowest air flowrate value selected for the experiments (90 $L.h^{-1}$) is slightly under the working recommendations of the nozzle provider. For this flowrate, results that are not fully process-driven might appear, explaining the high impact of the liquid physico-chemistry (through *Bo*) predicted by the model on $d_{v,50}$.

Considering the range of conditions studied, the model fitness is rather satisfactory, as it reasonably predicts the diameters over the whole range of conditions considered (52 over 75 points predicted in the 20% relative error range). However, the predicted value for diameters in the range 40-60 µm is almost systematically higher than the experimental value. This deviation indicates that the mathematical equation of the model cannot perfectly account for cases in which the resulting diameter is intermediate in size. The milk validation points (red dots) confirm this hypothesis: the quality of the prediction for these experiments is similar to model solutions in this diameter range. The model depicted by *Equation 7* also underpredicts the $d_{v,50}$ values over 100 µm when spraying milk, failing at seizing the complexity of interactions at stake for these operating conditions. The validation data set thus clearly reveals the limits of the model.

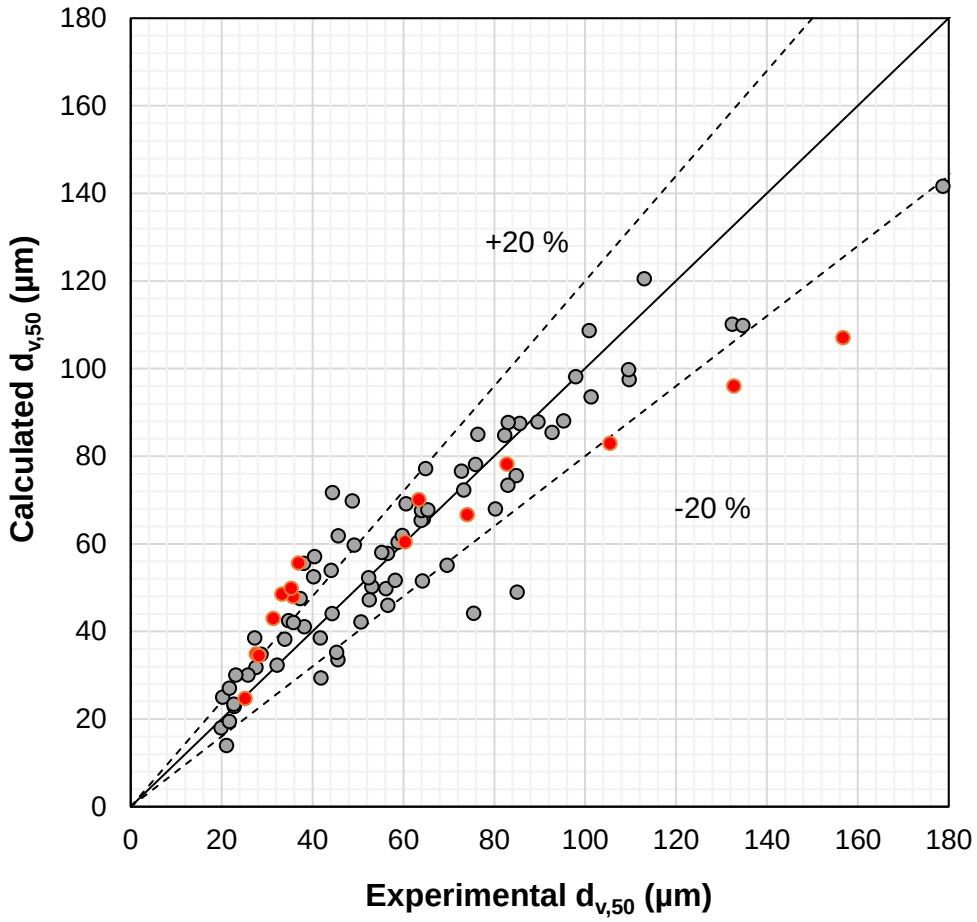

Figure 6: *Calculated vs. experimental $d_{v,50}$ for the conventional model*

The generation of a spray comes with three phenomena whose prevalence is highly dependent on the distance from the nozzle outlet. Following ligament formation, fine droplets are stripped from these ligaments, which then establishes coalescence/rupture equilibrium. Petit et al. [4] found that the higher the distance from the nozzle, the higher the impact of the physico-chemistry due to the contribution of coalescence to PSD. Whereas Petit et al. studied atomization at distances from the nozzle outlet of 5 and 14 cm, the data in this study was recorded closer to the nozzle outlet (1.5 cm). An unexpected consequence of this shorter distance is that our models consequently place significant importance on physico-chemistry. Our results thus prove that bifluid atomization is highly sensitive to the distance from the nozzle outlet, and researchers should take high precaution before applying a correlation from the literature in order to ensure reliable results.

Although the model introduced in *Equation 7* is generally satisfactory, it nevertheless has some apparent flaws. One of the most problematic flaws involves how the model overestimates sizes from the validation data set between 40-60 µm and underestimates them over 100 µm. Resolving this issue required identifiying a new model using the software Eureqa (accordingly to the procedure mentioned in *2.3.1)*. Among the equations proposed by the software, we chose the one offering the best fitting result while keeping the number of identified constants as low as possible for practical ease of use. *Equation 8* introduces the identified equation, and *Figure 7*: Calculated vs. experimental $d_{v,50}$ for the model identified with symbolic regression represents the accordance between experimental data and modelled diameters.

$\frac{d_{v,50}}{L} = 0.0002 * ALR + 2.5 * 10^{-7}.\frac{\mu_L}{\mu_A} + \frac{24.7 * Bo - 2.88}{0.013.\frac{\mu_L}{\mu_A} + We * ALR}$	*Equation 8*

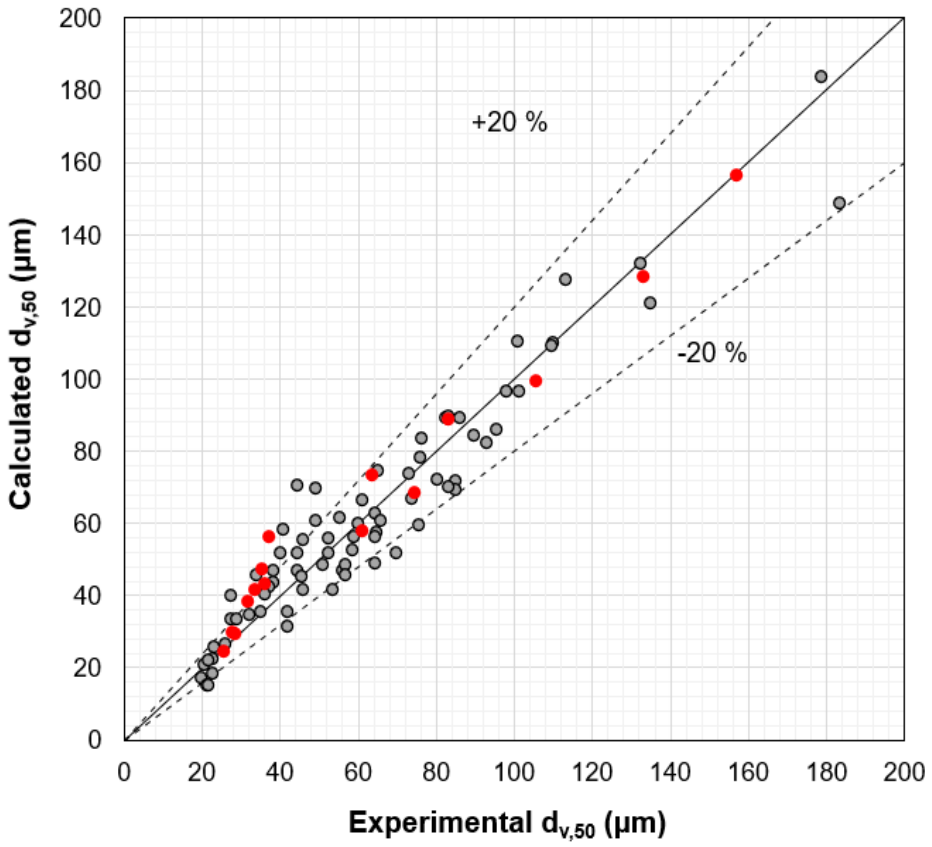

Figure 7: Calculated vs. experimental $d_{v,50}$ for the model identified with symbolic regression

The coefficient of correlation R^2 and the root-mean squared error *RMSE* calculated for this model are respectively R^2 = 0.92 and *RMSE* = 0.0006. 58 over 75 points for the training data are within the 20% relative error range. This new correlation thus clearly improves the overall quality prediction (higher R^2). The prediction deviations observed for the lower range of sizes are still present but dampened. The largest particles of the validation data set, which are poorly predicted with *Equation 7*, are now almost perfectly calculated by the model developed with the *Equation 8*.

As was the case in *Equation 7*, the density ratio remains insignificant in this model. This redundancy gives confidence to the notion that such insignificance is due to physical and experimental concerns and not related to the shape of the relation. The model depicted by *Equation 8* displays complex physio-chemical and process operating parameters interactions. The influence of the *Bo* number (gravitational forces to surface tension ones) and *We* number (aerodynamic forces to surface tension forces) should probably not be considered independently. These models also should include the viscous forces influence to offer a satisfactory prediction in a large range of diameters. The equation shape identified by the machine-learning approach offers an interesting representation of how physical properties can interact when spraying a fluid.

4.2 Average number diameter correlations

Under some conditions, estimating the average number diameter can also be of great interest. This diameter is usually introduced as the ratio between the moments of order 1 and 0 of the number PSD. *Equation 9* presents the monomial/exponential correlation identified from our experimental results with MATLAB for $d_{n,av}$.

$\frac{d_{n,av}}{L} = 2 * 10^{-9} * (Bo)^{0.48} * \left(\frac{\rho_L}{\rho_A}\right)^{2.11} * (ALR)^{-0.08} * e^{-9.8*10^{-5}*We}$	*Equation 9*

All the dimensionless numbers were found to be statistically significant (*p-values* > 0.05), with the exception of the viscosity ratio $\frac{\mu_L}{\mu_A}$. *Equation 9* was thus obtained after removing the viscosity ratio for the identification. The adjusted coefficient of correlation R^2 and the root mean square error *RMSE* for this modelling were respectively R^2 = 0.92 and *RMSE* = 0.00011. The adequacy between the experimental and model values is presented in *Figure* , and milk points are plotted with red dots.

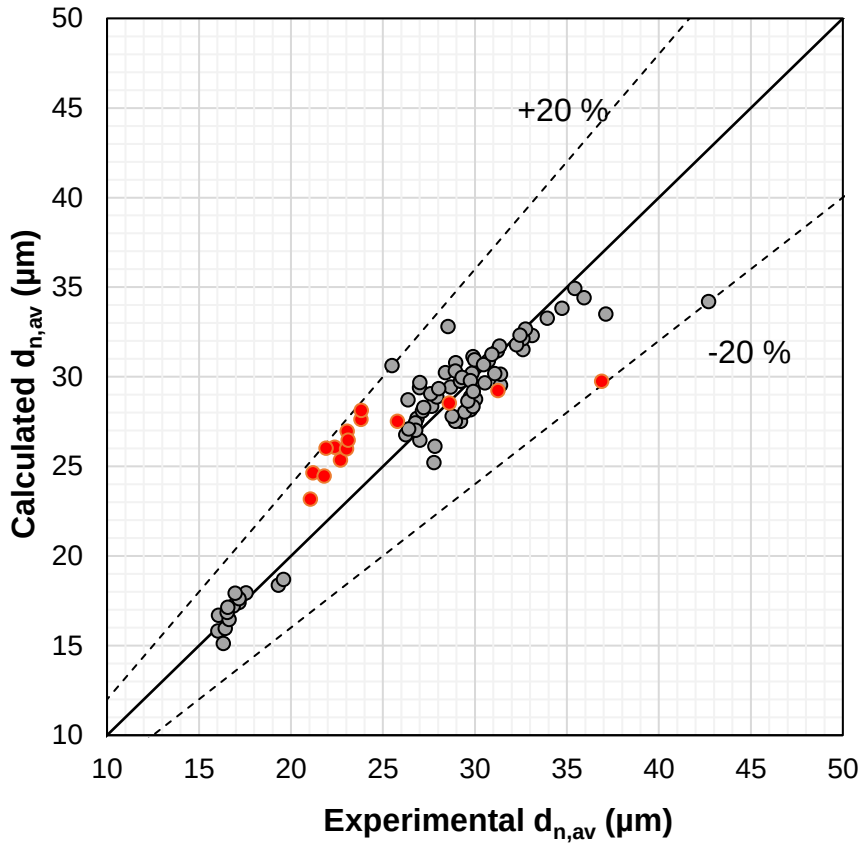

Figure 8: Calculated vs. experimental $d_{n,av}$ for the conventional model

The adjustment observed in *Figure 8: Calculated vs. experimental $d_{n,}$* is excellent, with 74 of the 75 experimental points predicted within the 20% relative interval and almost all the validation points lying within this interval. The validation data also seems correctly predicted, even though a deviation starts to be visible on the largest particles.

The use of the same monomial modelling structure for $d_{n,av}$ and $d_{v,50}$ also allows some points of comparison between the prevalence of the phenomena at stake by comparing the relative contribution of the dimensionless numbers considered to the estimated diameter. The *Bo* number and *ALR* influences are significantly less pronounced in this correlation, indicating some apparent differences with the previous case in the physical phenomena impacting $d_{n,av}$.

By choosing the estimation of a characteristic diameter like $d_{n,av}$ (related to a number distribution), the interactions between the physico-chemistry of the product and the process seem to be less complicated for simple monomial-exponential models to account for. An explanation could be that number distributions give significantly less importance to the largest particles than volume distributions, where a single large particle can have a massive impact on the distribution (as the volume is proportional to the size power three, assuming sphericity). Therefore, largest particles moderately impact characteristic diameters in the case number distributions. It would mean that complex physico-chemistry/process interactions mainly impact the largest particles, explaining the deviation observed for the "middle size" particles for $d_{v,50}$ models. This poor diameter prediction on midrange values could indeed be related to the fact that large median volumetric droplets hold significant importance when identifying the model, thus impacting the overall prediction quality of median volumetric diameter.

As we previously did for $d_{v,50}$, a symbolic regression correlation was also searched for $d_{n,av}$ using the software Eureqa considering all the dimensionless numbers established by the dimensional analysis. The equation obtained is presented in *Equation 10*, while the graphical representation of the prediction for trained and validation data sets is shown in *Figure* .

$\frac{d_{n,av}}{L} = 0.0046 + 3.9 * 10^{-5} * Bo * \frac{\rho_L}{\rho_A} + \frac{11{,}4 * Bo^3}{We * ALR} - 3.5 * 10^{-6} * \frac{\rho_L}{\rho_A} - 0.036 * Bo$	*Equation 10*

For this model, R^2 = 0.93 and the *RMSE* = 0.00010; 73 points over 75 are predicted in the 20% error interval. The software also found the viscosity ratio to be insignificant for the $d_{n,av}$ prediction, as was the case with the conventional model. As seen in *Figure* , the viscosity ratio interval considered is rather large; the magnitude of the values considered is thus unlikely to explain this insignificance, which is thus most likely due to the physics of the phenomena involved. The overall quality prediction for the trained data is very similar to the one obtained with *Equation 9*. However, clear differences are observed when considering the validation data set: the 20-30 µm points are now almost perfectly predicted, while a lesser deviation is observed for the largest particles.

When observing the shape of the relation proposed by Eureqa, it seems that *We* is only involved inside an interaction term somewhat similar to the one obtained with *Equation 8*, with *Bo* on the numerator and *We*ALR* on the denominator. This interesting fact thus gives some leads on how to accurately account for the impact of the interactions while modelling an atomization characteristic diameter.

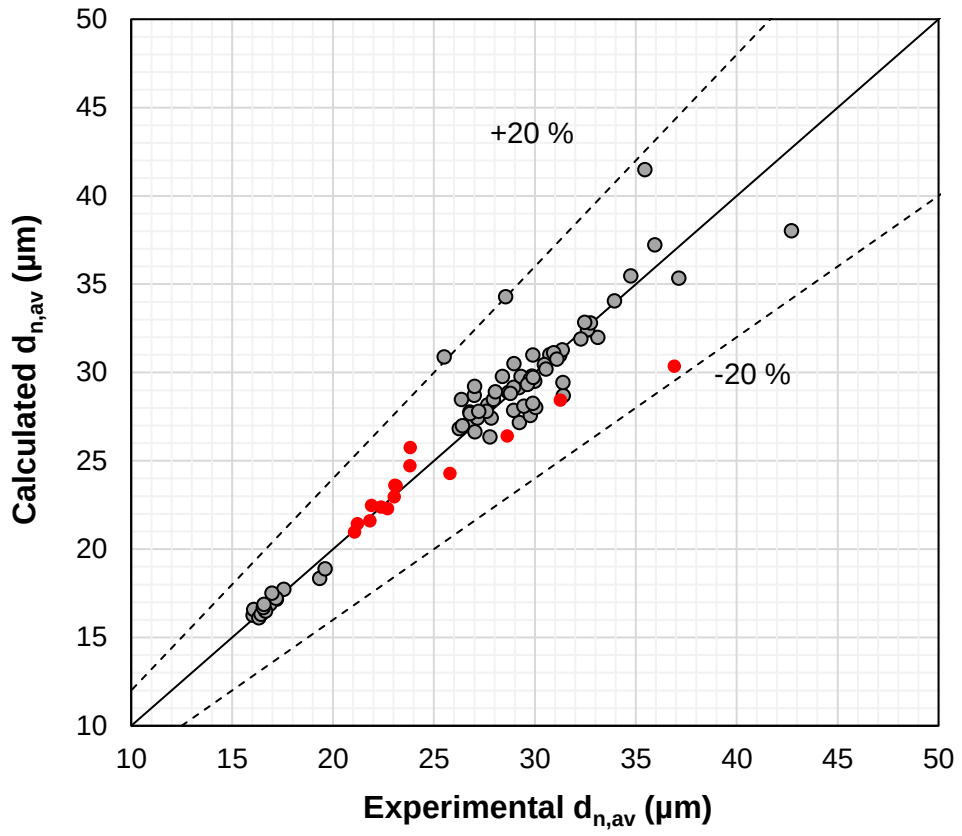

Figure 9: Calculated vs. experimental $d_{n,av}$ for the model identified with symbolic regression

Based on the models obtained for $d_{v,50}$ and $d_{n,av}$, some general guidelines can be drawn. While the simple monomial/exponential relations were satisfactory overall, the ones obtained through a machine-learning approach were systematically more accurate while keeping the same number of parameters (5 in total) to be adjusted. The comparison between the relations also highlighted that depending on the distribution considered (number or volume), the physical phenomena at stake would not have the same impact on the final property estimation, probably due to the relative accountancy of the largest droplets of the distribution. The formulas proposed by the machine-learning approach thus highlighted some way to better seize these complex interactions from a numerical point of view. The comparison between the diameters and the methods (conventional and symbolic regression) thus offers an interesting way to make atomization modelling more complex while shedding some light on the physical interactions at stake.

4.3 Particle Size Distribution modelling

4.3.1 The physics of sprays and jets

Liquid fragmentation is a long-time studied physical phenomenon that continues to fascinate engineers and physicists [22–25]. Recent studies of Villermaux et al. [15,23,26] shed light on the mechanisms involved during coaxial liquid atomization, and proposed a fragmentation theory known as ligament-mediated spray theory. Their theoretical background remains used in recent atomization modelling research [22,25]. According to this theory, when sprayed, the liquid bulk undergoes

instabilities due to shearing at the liquid/gas interface (Kelvin-Helmholtz type, then Raileigh-Taylor when the amplitude of the first waves is large enough). These Rayleigh-Taylor instabilities combined with the influence of the air flow generate ligaments (elongated liquid fractions stemming from the bulk due to the surface disturbances), which are comprised of elements called blobs.

Villermaux [15] showed that the distribution of these blobs follows a fragmentation-coalescence dynamics, which number probability distribution can be described with a Gamma distribution such as (*Equation 11*):

$P\left(x = \frac{d}{d_{n,av}}\right) = \mathbb{\Gamma}(n,x) = \left[\frac{n^n}{\mathbb{\Gamma}(n)}\right] x^{n-1} e^{-nx}$	*Equation 11*

Where $d_{n,av}$ is the average number diameter of the blob distribution and *n* is a parameter indicating the broadness of the distribution: the lower is *n*, the broader is the distribution (*Figure 10*). Villermaux successfully fitted this distribution shape to the droplets stripped from the ligaments, validating its relevance in the case of bifluid atomization. However, for some atomization conditions, a significant ligament population can also appear in the final spray distribution. In that case, the final spray distribution is a convolution of the large ligament distribution and small droplets distribution, resulting in an exponential tail displaying the same *n* value as the blob distribution.

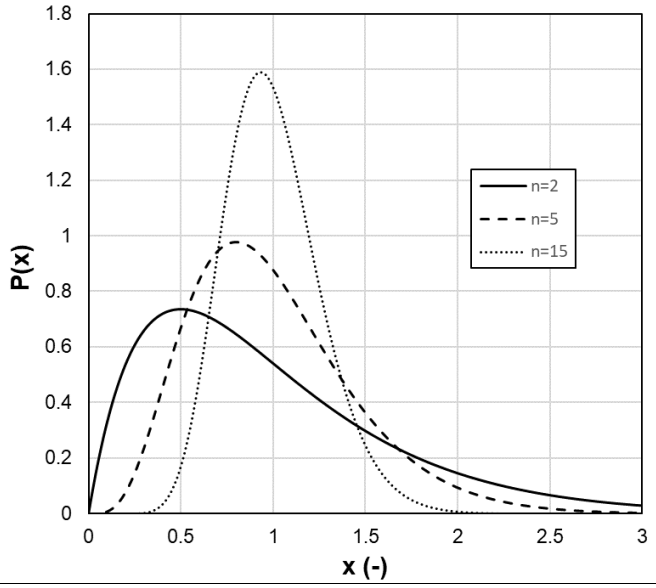

Figure 10: Gamma distribution for various n values.

4.3.2 Adequation of the Gamma function to the experimental droplet size distributions

Two parameters appear in *Equation 11*: the average number diameter of the distribution $d_{n,av}$ and the polydispersity index *n*. $d_{n,av}$ is also the ratio between the first-order moment and zero-order moment of the distribution, and is thus easy to estimate knowing the diameter of each droplet. After estimating $d_{n,av}$, *n* is adjusted by fitting the numerical integral of the Gamma function to the cumulative distribution experimentally obtained through a least-squares optimization. By defining *p* as the number of the droplet considered (sorted by increasing size), p_{tot} as the total number of droplets considered and x_p as the normalized particle size related to the particle *p*, the least-squares function numerically assessed is described by *Equation 12*:

$$LS = min\left[\sum_{p=1}^{p_{tot}}\left(\frac{p}{p_{tot}} - \int_0^{x_p}\left[\frac{n^n}{\mathbb{\Gamma}(n)}\right]{x_p}^{n-1}e^{-n.x_p}\,.\,dx_p\right)^2\right] \qquad \textit{Equation 12}$$

The results obtained for two different experimental conditions (sprayed solution 1) are represented in *Figure 1*. The experimental distributions (dashed lines) were reconstituted from the cumulative experimental data by linearly interpolating the results over 1000 equidistant points relatively to size (*interp1* function), then numerically differentiating the interpolated data (*diff* function). Modelled distributions were obtained by plotting *Equation 11* with the value of *n* optimized through least-squares function minimization computed by *Equation 12*.

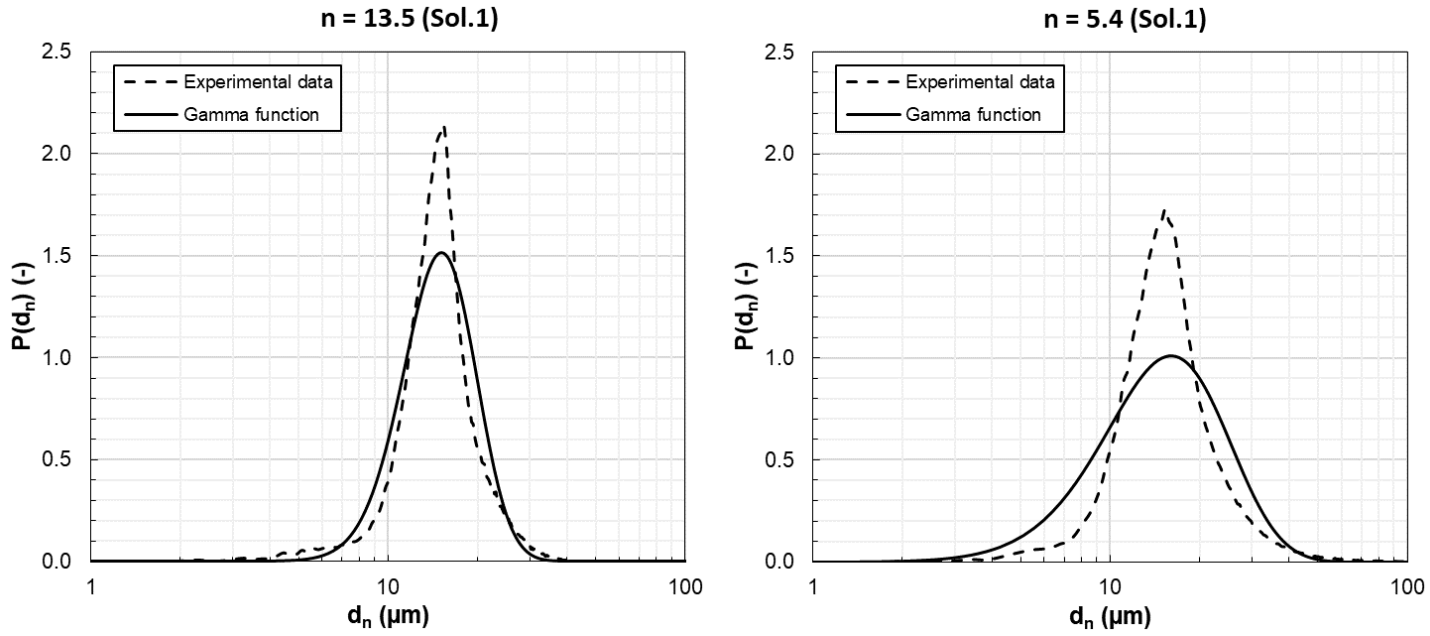

Figure 11: Experimental distribution (dashed line) and Gamma function (solid line) for two spraying conditions with solution 1

The agreement between the experimental distribution and the theoretical function is good for large *n* values (left graph, *n* = 13.5). While the peak height is underestimated, the Gamma function accounts well for the global shape of the distribution. More precautions should be taken when using the Gamma function for small *n* values, as the function clearly tends to overestimate the probability distribution in

the regions near the peak while underestimating its intensity. This result is actually expected, since it has been reported elsewhere [22,27]. More precisely, it is mentioned that when the ligament distribution is narrowly distributed inside the droplet population (corresponding to large *n* values), *Equation 11* is indeed suited to describe the spray distribution. Nevertheless, for cases in which air momentum is such as the ligaments exhibits more corrugation, the global size distribution tends to turn into an incomplete Gamma function. Also, the shape of the distribution can be considered relatively simple (2 fitting parameters) considering the complexity of the physical phenomena involved (air shearing, entrainment, coalescence, and rupture). 3-parameters PSD functions are usually more efficient in taking into account both the maximal height of the peak and the polydispersity in the case of atomization [28]. However, these functions could not be recommended for this study, since the primary goal is to provide the experimentalist a quick way to assess a size distribution over an extensive range of experimental conditions. A fast estimation of *n* is interesting to estimate the relevance of using the simple two-parameters approach proposed in this study. For small *n* values, the reconstitution of the distribution should be carefully managed, and more complex modelling options should be considered.

4.3.3 Determining a correlation for n

The physical parameters impacting the characteristic diameter will also impact the polydispersity index *n*, which is a dimensionless number. The dimensionless numbers quantifying the dimensionless characteristic diameter are thus also relevant for modelling *n*. A first attempt to identify *n* through a monomial equation was performed, which is shown in *Equation 13*.

$n = a_0.(Bo)^{a_1}.\left(\frac{\mu_L}{\mu_A}\right)^{a_2}.(ALR)^{a_3}.(We)^{a_4}.\left(\frac{\rho_L}{\rho_A}\right)^{a_5}$	*Equation 13*

After removing the non-significant parameters, the coefficient of correlation between the model/experiment and the root mean-squared error were calculated and found to be R^2 = 0.57 and *RMSE* = 2.09. The monomial form is thus unable to account for the complex interaction parameters at stake in the polydispersity of the system, and is not recommended to estimate *n*.

The use of a machine-learning approach is especially relevant here. The equation obtained with the software Eureqa is presented in *Equation 14*, and the graphical representation of the adequation between the experimental results and the model is shown in *Figure 32*: Calculated vs. experimental n for the model identified with symbolic regression*2*.

$n = 16.4 + 0.012 * \frac{\mu_L}{\mu_A} + 0.027 * Bo * We - \frac{32.2 * Bo}{Bo + ALR} - 32.87 * Bo - 1.4 * 10^{-6} * We * \frac{\mu_L}{\mu_A}$	*Equation 14*

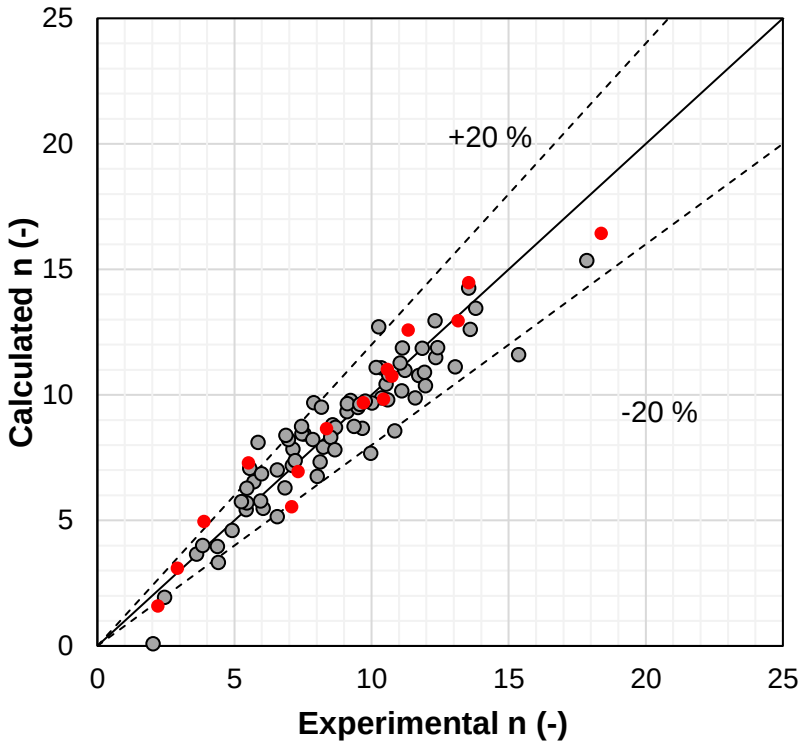

Figure 32: Calculated vs. experimental n for the model identified with symbolic regression

For this correlation, R^2=0.87, and the *RMSE* is of 1.1. 67 of the 75 points of the training data are in the 20% relative error interval. The obtained model can be considered to be good, as it correctly predicts the value of *n* for the validation data set. The shape of *Equation 14* clearly exhibits strong interaction terms accounting for the cases in which the polydispersity is not fully process-driven. We can observe that the higher the value of the process parameters (mainly air velocity), the higher the value of *ALR* and *We* number and the higher the value of *n*, indicating a lesser polydispersity (*Bo*We* and $\frac{Bo}{Bo+ALR}$). This influence is however attenuated by the viscous forces, which can be expected to exert some resistance to the air shearing, and thus increase the polydispersity (lowering *n*): the term $We * \frac{\mu_L}{\mu_A}$ is indeed negative. These interpretations should be carefully considered, as the dimensionless numbers do not account for one single effect (as for example, surface tension is also part of the Weber number). However, this equation and these interpretations give key parameters governing the phenomena to account for when modelling polydispersity and some guidance about the way to simply consider complex interactions for atomization.

4.3.4. Particle size distribution prediction

The prediction quality of the PSD modelling was then tested by using the previously established models. Firstly, the prediction of *n* by *Equation 14* was used in combination with the Gamma function (*Equation 12*) to predict the normalized number PSD for milk spraying (validation data set). Two results, corresponding to calculated *n* values respectively equal to 13.2 and 18.4 are presented in *Figure 43*: Experimental and predicted Gamma functions for milk*3.*

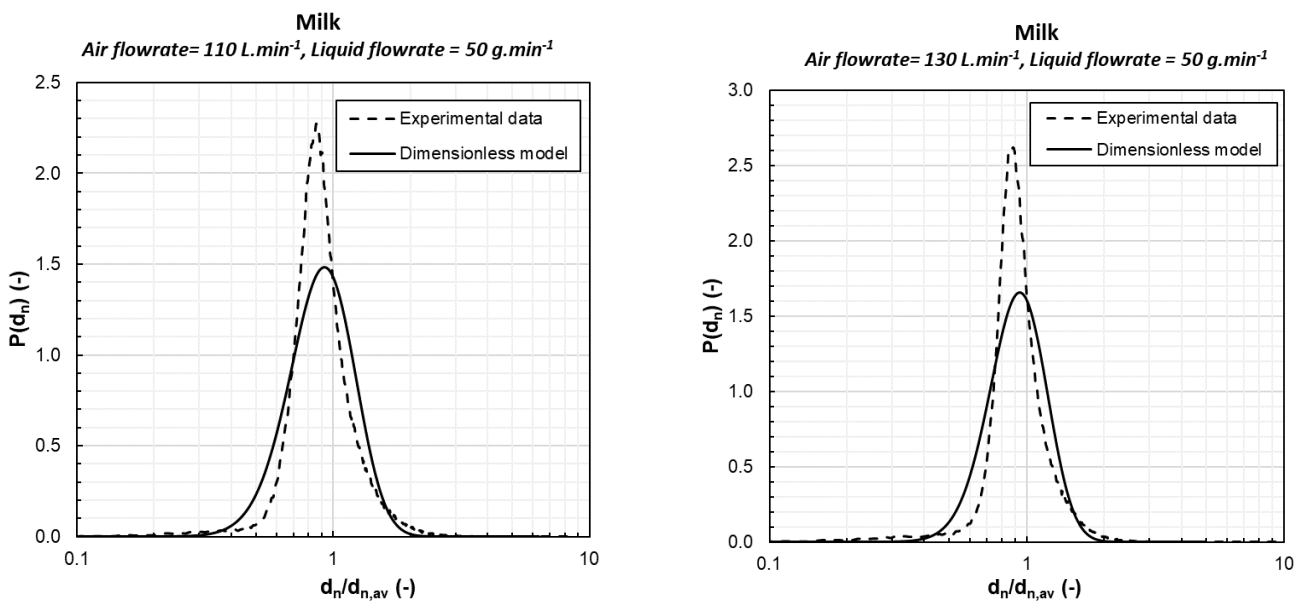

Figure 43: Experimental and predicted Gamma functions for milk

Figure 43 shows that the quality of the model for the normalized distribution is similar to the one found when assessing the relevance of using the Gamma function (*Figure*): the overall distribution shape is seized by the model, but the main peak intensity is underpredicted. In the case of milk, for high *n* numbers, both the shape of the distribution and the *n* prediction are thus relevant to have an indication about the expected size distribution when atomizing the solution. For low *n* values (not represented here), the same behavior as in *Figure* was observed. In these cases, while the value of *n* is a precious indication of polydispersity degree that can be expected, distribution reconstitution should be processed with care.

The real number PSD were also fully reconstructed using the $d_{n,av}$ modelled (*Equation 10*) inside the Gamma function. The results obtained for the same conditions as earlier are plotted in *Figure 54*. The addition of this model does not have a significant impact on the global quality of the model: no significant diameter offset of the main mode is indeed observed. For the reconstruction performed, the quality of the $d_{n,av}$ and *n* models obtained with machine-learning is thus satisfactory enough not to degrade the Gamma function quality of prediction. While not perfect, this attempt of reconstituting a full PSD based on simple correlations shows what can be expected from such relations and gives some solid leads for improvement.

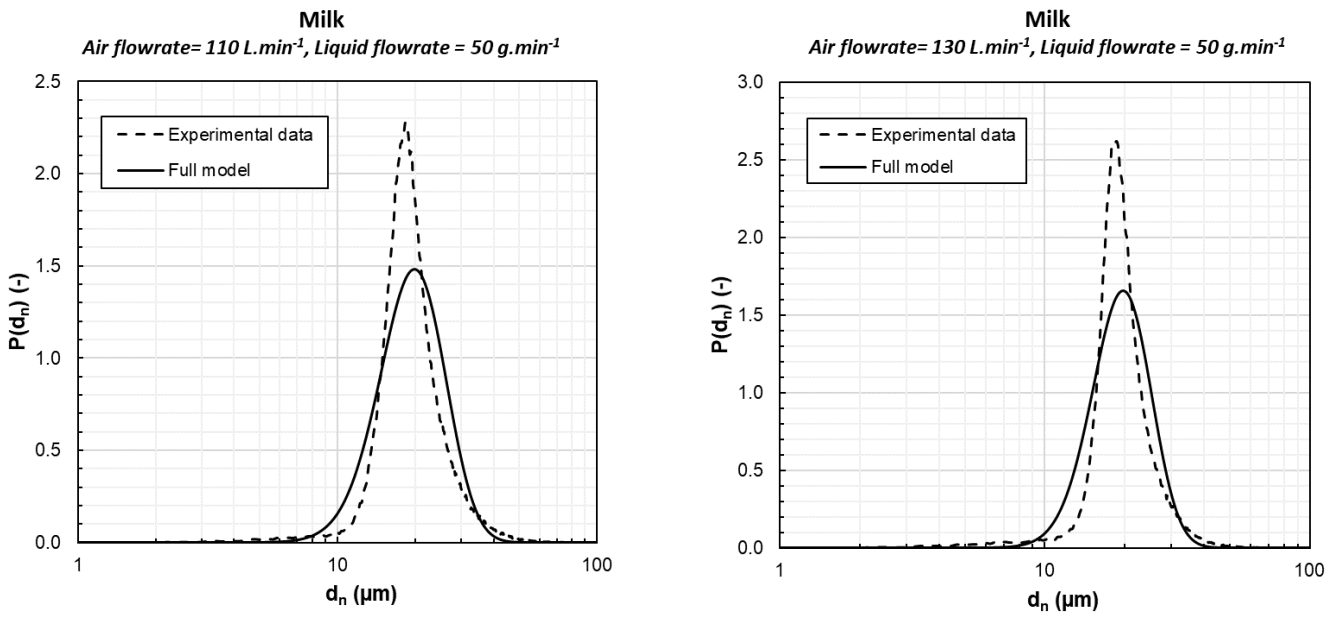

Figure 54: Size distribution prediction for two milk spraying conditions

Conclusion

The modelling of complex physical phenomena often involves high complexity in the applied mathematical approach. Atomization is no exception to that, as both process conditions and physico-chemistry have a significant impact on the shearing, coalescence, and rupture phenomena involved.

Using a rigorous dimensional analysis methodology, this article explores a way to model characteristic diameters related to volume and number distributions in the case of bifluid nozzle atomization. More precisely, two models are proposed per diameter: one based on the conventional monomial/exponential function shape and the other one obtained identifying a relation between relevant dimensionless numbers using a machine-learning software. The models found with the symbolic regression approach predict the droplet diameters for the milk validation data set systematically better. However, while some clear limitations are visible for the conventional models, they can overall be qualified as good. Comparing the models' terms for the two diameters also allowed to see that, depending on the distribution type (volume or number), the phenomena involved do not have the same impact on the characteristic diameter, possibly due to the magnitude of the contribution of the largest particles.

A methodology is also proposed to estimate a number PSD, based on the fragmentation theory introduced by Villermaux [15]. The identification of a correlation relating the polydispersity index *n* to the process parameters indeed allows, through the use of a Gamma function, to predict number PSD for milk spraying. The distribution reconstruction at large *n* values is overall satisfactory while the PSD prediction at low *n* numbers is more questionable (due to the Gamma function relevance itself more than to the models accuracy). However, the value of *n* in itself contains very interesting information about the polydispersity that can be expected, and the need or not to consider a more complex modelling.

Acknowledgements

The authors would like to thank Soredab for funding the internship of Mamadou Lamine Niane.

Nomenclature

Bo	Bond number (-)
$d_{a,int}$	Internal diameter for air section(m)
$d_{a,ext}$	External diameter for air section (m)
d_{char}	Characteristic droplet diameter (m)
d_l	Internal diameter for liquid section (m)
$d_{n,av}$	Average number diameter (m)
$d_{v,50}$	Median volumetric diameter (m)
f	Process function (with dimensions) (-)
F	Dimensionless process function (-)
L	Distance of the observation zone to the nozzle outlet (m)
$\dot{m}$	Mass flowrate (kg.m^{-3})
n	Probability distribution parameter (-)
p	Droplet number (-)
p_{tot}	Total droplet numbers for a sprayed condition (-)
u	Average velocity (m.s^{-1})
V	Tank volume (m^3)
We	Weber number (-)
x	Normalized droplet size (-)

Greek letters

ξ	Ligament thickness before breakup (m)
μ	Dynamic viscosity (Pa.s)
σ	Surface tension (N.m^{-1})
ρ	Density (kg.m^{-3})

Abbreviations

ALR	Air-to-Liquid Ratio (-)
DA	Dimensional Analysis
LS	Least-Squares function (-)
ML	Machine-learning
MMD	Mass Median Diameter (m)
PSD	Particle Size Distribution
RMSE	Root-Mean-Square Error (-)

References

[1] G.M. Faeth, Current status of droplet and liquid combustion, Prog. Energy Combust. Sci. 3 (1977) 191–224.
[2] J. Guerin, J. Petit, J. Burgain, F. Borges, B. Bhandari, C. Perroud, S. Desobry, J. Scher, C. Gaiani, Lactobacillus rhamnosus GG encapsulation by spray-drying: Milk proteins clotting control to produce innovative matrices, Journal of Food Engineering. 193 (2017) 10–19. https://doi.org/10.1016/j.jfoodeng.2016.08.008.
[3] K. Lachin, C. Turchiuli, V. Pistre, G. Cuvelier, S. Mezdour, F. Ducept, Dimensional analysis modeling of spraying operation – Impact of fluid properties and pressure nozzle geometric parameters on the pressure-flow rate relationship, Chemical Engineering Research and Design. 163 (2020) 36–46. https://doi.org/10.1016/j.cherd.2020.08.004.
[4] J. Petit, S. Méjean, P. Accart, L. Galet, P. Schuck, C. Le Floch-Fouéré, G. Delaplace, R. Jeantet, A dimensional analysis approach for modelling the size of droplets formed by bi-fluid atomisation, Journal of Food Engineering. 149 (2015) 237–247. https://doi.org/10.1016/j.jfoodeng.2014.10.022.
[5] M. Suzuki, H. Sato, M. Hasegawa, M. Hirota, Effect of size distribution on tapping properties of fine powder, Powder Technology. 118 (2001) 53–57. https://doi.org/10.1016/S0032-5910(01)00294-7.
[6] S. Mandato, E. Rondet, G. Delaplace, A. Barkouti, L. Galet, P. Accart, T. Ruiz, B. Cuq, Liquids' atomization with two different nozzles: Modeling of the effects of some processing and formulation conditions by dimensional analysis, Powder Technology. 224 (2012) 323–330.
[7] J. Ballester, C. Dopazo, Drop size measurements in heavy oil sprays from pressure-swirl nozzles, Atomization and Sprays. 6 (1996) 377–408. https://doi.org/10.1615/AtomizSpr.v6.i4.10.
[8] A.J. Hewitt, Droplet size spectra produced by air-assisted atomizers, Journal of Aerosol Science. 24 (1993) 155–162.
[9] C.-C. Chu, S.-F. Chou, H.-I. Lin, Y.-H. Liann, An experimental investigation of swirl atomizer sprays, Heat and Mass Transfer. 45 (2008) 11–22. https://doi.org/10.1007/s00231-008-0389-1.
[10] P. Somasundaran, V. Runkana, Modeling flocculation of colloidal mineral suspensions using population balances, International Journal of Mineral Processing. 72 (2003) 33–55.
[11] B. Zhang, L. Kong, H. Jin, G. He, S. Yang, X. Guo, CFD simulation of gas–liquid flow in a high-pressure bubble column with a modified population balance model, Chinese Journal of Chemical Engineering. 26 (2018) 1350–1358. https://doi.org/10.1016/j.cjche.2018.01.003.
[12] R. Hassan, K. Loubiere, J. Legrand, G. Delaplace, A consistent dimensional analysis of gas-liquid mass transfer in an aerated stirred tank containing purely viscous fluids with shear-thinning properties, Chemical Engineering Journal. 184 (2012) 42–56. https://doi.org/10.1016/j.cej.2011.12.066.
[13] G. Delaplace, Y. Gu, M. Liu, R. Jeantet, J. Xiao, X.D. Chen, Homogenization of liquids inside a new soft elastic reactor: Revealing mixing behavior through dimensional analysis, Chemical Engineering Science. 192 (2018) 1071–1080. https://doi.org/10.1016/j.ces.2018.08.023.
[14] A. Berth, D. Lecouturier, K. Loubiere, P. Dhulster, G. Delaplace, Modelling and optimisation of gas-liquid mass transfer in a microporous hollow fiber membrane aerated bioreactor used to produce surfactin, Biochemical Engineering Journal. 145 (2019) 109–119. https://doi.org/10.1016/j.bej.2018.10.029.
[15] E. Villermaux, Ph. Marmottant, J. Duplat, Ligament-Mediated Spray Formation, Physical Review Letters. 92 (2004). https://doi.org/10.1103/PhysRevLett.92.074501.
[16] G. Delaplace, K. Loubière, F. Ducept, R. Jeantet, Dimensional analysis of food processes, ISTE Press, Elsevier, 2015.
[17] A.H. Lefebvre, V.G. McDonell, Atomization and sprays, Second edition, CRC Press, Taylor & Francis, Boca Raton, 2017.
[18] S. Poozesh, N. Setiawan, N.K. Akafuah, K. Saito, P.J. Marsac, Assessment of predictive models for characterizing the atomization process in a spray dryer's bi-fluid nozzle, Chemical Engineering Science. 180 (2018) 42–51. https://doi.org/10.1016/j.ces.2018.01.033.

[19] W.H. Hager, Wilfrid Noel Bond and the Bond number, Journal of Hydraulic Research. 50 (2012) 3–9. https://doi.org/10.1080/00221686.2011.649839.
[20] R. Bois, O. Adriao, G. Delaplace, I. Pezron, A. Nesterenko, E. van-Hecke, Influence of process variables on foaming ability of surfactants: Experimental study and dimensional analysis, Chemical Engineering Research and Design. 165 (2021) 40–50. https://doi.org/10.1016/j.cherd.2020.10.021.
[21] A.S. Bongo Njeng, S. Vitu, M. Clausse, J.-L. Dirion, M. Debacq, Effect of lifter shape and operating parameters on the flow of materials in a pilot rotary kiln: Part III. Up-scaling considerations and segregation analysis, Powder Technology. 297 (2016) 415–428. https://doi.org/10.1016/j.powtec.2016.04.052.
[22] B. Keshavarz, E.C. Houze, J.R. Moore, M.R. Koerner, G.H. McKinley, Ligament Mediated Fragmentation of Viscoelastic Liquids, Physical Review Letters. 117 (2016). https://doi.org/10.1103/PhysRevLett.117.154502.
[23] J. Eggers, E. Villermaux, Physics of liquid jets, Reports on Progress in Physics. 71 (2008) 036601. https://doi.org/10.1088/0034-4885/71/3/036601.
[24] L. Liu, Q. Fu, L. Yang, Theoretical atomization model of liquid sheet generated by coaxial swirl injectors, International Journal of Multiphase Flow. 142 (2021) 103725. https://doi.org/10.1016/j.ijmultiphaseflow.2021.103725.
[25] Z. Xu, H. Zhao, H. Liu, Atomization model based on the ligament-mediated spray mechanism for coaxial two-fluid air-blast nozzle, Chemical Engineering Journal. 450 (2022) 137986. https://doi.org/10.1016/j.cej.2022.137986.
[26] E. Villermaux, Fragmentation, Annu. Rev. Fluid Mech. 39 (2007) 419–446.
[27] P. Marmottant, E. Villermaux, On spray formation, J. Fluid Mech. 498 (2004) 73–111. https://doi.org/10.1017/S0022112003006529.
[28] A. Urbán, A. Groniewsky, M. Malý, V. Józsa, J. Jedelský, Application of big data analysis technique on high-velocity airblast atomization: Searching for optimum probability density function, Fuel. 273 (2020) 117792. https://doi.org/10.1016/j.fuel.2020.117792.